Retinal OCT-Derived Texture Features as Potential Biomarkers for Early Diagnosis and Progression of Diabetic Retinopathy

Sara Oliveira,[1–3] Pedro Guimarães,[3–5] Elisa Julião Campos,[1–3,6,7] Rosa Fernandes,[1–3,8] João Martins,[4] Miguel Castelo-Branco,[3–5] Pedro Serranho,[4,9] Paulo Matafome,[1–3,10,11] Rui Bernardes,[3–5] and António Francisco Ambrósio[1–3]

[1]University of Coimbra, Coimbra Institute for Clinical and Biomedical Research (iCBR), Faculty of Medicine, Coimbra, Portugal
[2]University of Coimbra, Center for Innovative Biomedicine and Biotechnology (CIBB), Coimbra, Portugal
[3]Clinical Academic Center of Coimbra (CACC), Coimbra, Portugal
[4]University of Coimbra, Coimbra Institute for Biomedical Imaging and Translational Research (CIBIT), Institute for Nuclear Sciences Applied to Health (ICNAS), Coimbra, Portugal
[5]University of Coimbra, Faculty of Medicine (FMUC), Coimbra, Portugal
[6]University of Coimbra, Chemical Engineering and Renewable Resources for Sustainability (CERES), Department of Chemical Engineering (DEQ), Faculty of Sciences and Technology (FCTUC), Coimbra, Portugal
[7]University of Coimbra, Center for Neuroscience and Cell Biology (CNC-UC), Coimbra, Portugal
[8]University of Coimbra, Institute of Pharmacology and Experimental Therapeutics, Faculty of Medicine, Coimbra, Portugal
[9]Universidade Aberta, Department of Sciences and Technology, Lisbon, Portugal
[10]University of Coimbra, Institute of Physiology, Faculty of Medicine, Coimbra, Portugal
[11]Polytechnic University of Coimbra, Health and Technology Research Center (H&TRC), Coimbra Health School (ESTeSC), Coimbra, Portugal

Correspondence: António Francisco Ambrósio, University of Coimbra, Coimbra Institute for Clinical and Biomedical Research (iCBR), Faculty of Medicine, Polo III - Health Sciences Campus, Azinhaga de Santa Comba, Coimbra 3000-548, Portugal; afambrosio@fmed.uc.pt.
Rui Bernardes, University of Coimbra, Coimbra Institute for Biomedical Imaging and Translational Research (CIBIT), Institute for Nuclear Sciences Applied to Health (ICNAS), Polo III - Health Sciences Campus, Azinhaga de Santa Comba, Coimbra 3000-548, Portugal; rmbernardes@fmed.uc.pt.
Sara Oliveira, University of Coimbra, Coimbra Institute for Clinical and Biomedical Research (iCBR), Faculty of Medicine, Polo III - Health Sciences Campus, Azinhaga de Santa Comba, Coimbra 3000-548, Portugal; saraoliveira116@gmail.com.

RB and AFA contributed equally to this work.

Received: August 2, 2024
Accepted: November 29, 2024
Published: January 6, 2025

Citation: Oliveira S, Guimarães P, Campos EJ, et al. Retinal OCT-derived texture features as potential biomarkers for early diagnosis and progression of diabetic retinopathy. *Invest Ophthalmol Vis Sci.* 2025;66(1):7. https://doi.org/10.1167/iovs.66.1.7

Purpose. Diabetic retinopathy (DR) is usually diagnosed many years after diabetes onset. Indeed, an early diagnosis of DR remains a notable challenge, and, thus, developing novel approaches for earlier disease detection is of utmost importance. We aim to explore the potential of texture analysis of optical coherence tomography (OCT) retinal images in detecting retinal changes in streptozotocin (STZ)-induced diabetic animals at "silent" disease stages when early retinal molecular and cellular changes that cannot be clinically detectable are already occurring.

Methods. Volume OCT scans and electroretinograms were acquired before and 1, 2, and 4 weeks after diabetes induction. Automated OCT image segmentation was performed, followed by retinal thickness and texture analysis. Blood-retinal barrier breakdown, glial reactivity, and neuroinflammation were also assessed.

Results. Type 1 diabetes induced significant early changes in several texture metrics. At week 4 of diabetes, autocorrelation, correlation, homogeneity, information measure of correlation II (IMCII), inverse difference moment normalized (IDN), inverse difference normalized (INN), and sum average texture metrics decreased in all retinal layers. Similar effects were observed for correlation, homogeneity, IMCII, IDN, and INN at week 2. Moreover, the values of those seven-texture metrics described above decreased throughout the disease progression. In diabetic animals, subtle retinal thinning and impaired retinal function were detected, as well as an increase in the number of Iba1-positive cells (microglia/macrophages) and a subtle decrease in the tight junction protein immunoreactivity, which did not induce any physiologically relevant effect on the blood-retinal barrier.

Conclusions. The effects of diabetes on the retina can be spotted through retinal texture analysis in the early stages of the disease. Changes in retinal texture are concomitant with biological retinal changes, thus unlocking the potential of texture analysis for the early diagnosis of DR. However, this requires to be proven in clinical studies.

Keywords: diabetic retinopathy (DR), early biomarkers, optical coherence tomography (OCT), texture analysis

iovs.arvojournals.org | ISSN: 1552-5783

Diabetic retinopathy (DR) is one of the most frequent complications of diabetes mellitus (DM) and remains the primary cause of vision loss in working-age adults.[1] In the last 2 decades, knowledge gathered from basic and clinical research has changed our perspective on DR pathophysiology. The disease is increasingly recognized as a neurovascular disease, affecting both retinal microvasculature and neural cells, and as a low-grade chronic neuroinflammatory disease.[2–5] Despite advances in DR screening and treatment, the diagnostic resources currently available in clinical practice (color fundus retinal photography, ultra-widefield color fundus retinal photography, fluorescein angiography, ultra-widefield fluorescein angiography, optical coherence tomography (OCT), and angio-OCT) are not sensitive enough to detect early molecular and cellular changes in the retina. Early diagnosis of DR remains a major challenge due to the large time gap between diabetes onset and the detection of the first clinical signs of DR,[6] which is usually diagnosed when irreversible changes have already occurred in the retina. Therefore, identifying strategies for an earlier diagnosis is of utmost importance and useful for the timely recognition and management of high-risk individuals, allowing for closer follow-up and personalized screening.

The advent of OCT was a breakthrough in the field of ophthalmology, providing noninvasive, rapid, high-resolution, and real-time cross-sectional imaging of the retina.[7,8] In addition to its conventional use to assess changes in retinal morphology and thickness, several research groups have been presenting new applications of OCT to extract more in-depth information,[9–14] including our group.[15–21] Moreover, our team's work also involved the development of a new methodology based on texture analysis of OCT data.[22–25] As a proof of concept, we carried out a preclinical study with a transgenic mouse model of Alzheimer's disease and the corresponding wild-type mice. We were able to identify significant differences in the retinal texture at early stages of the pathology, as well as differences throughout the disease's progression.[22] This methodology was also applied in a clinical study in which it was possible, using classification models, to discriminate between patients diagnosed with Alzheimer's or Parkinson's disease and healthy controls.[23] These findings opened new avenues for identifying biomarkers, not only for brain neurodegenerative diseases but also for retinal degenerative diseases, based on OCT retinal texture.

In the present study, texture analysis was applied for the first time in the context of DR to assess early changes in retinal texture, potentially at disease stages that would not be clinically detectable, and to evaluate how retinal texture changes throughout the disease. Moreover, this study also sought to evaluate whether the changes in retinal texture were concomitant, or not, with molecular, cellular, vascular, and physiological alterations in the retina. Therefore, the main goal of this research study was to provide strong evidence for developing a texture-based approach capable of identifying retinal texture changes at very early "silent" disease stages when early molecular and cellular retinal changes that are not clinically detectable are already occurring. For this purpose, we carried out a longitudinal study using a widespread model of experimental type 1 diabetes, streptozotocin (STZ)-induced diabetes in Wistar Han rats (male and female rats), in which OCT acquisitions, electroretinography (ERG), and molecular, cellular, and vascular studies were performed. The gray-level co-occurrence matrix (GLCM) provides a statistical distribution of gray levels in an image and was used in this work to assess texture from OCT-derived images of rat retinas.

Animal models are fundamental for studying the retina because they allow the assessment of biological parameters that cannot be assessed in humans, thus providing an indispensable tool for better understanding the pathophysiology of retinal diseases and for the development of new therapies and diagnostic strategies for eye disorders. Although there are no animal models of diabetes that completely recapitulate all characteristics of human DR, studies conducted with the animal model used in this study (STZ-induced diabetic rats) reported multiple DR features, such as damaged/decreased pericytes and endothelial cells, increased acellular capillaries, basement membrane thickening, blood-retinal barrier breakdown, and loss of retinal ganglion cells.[26–29]

The use of an animal model in this study was crucial to clarify whether the potential changes in retinal texture are concomitant, or not, with subtle molecular and cellular alterations in the retina that have been linked to DR. Moreover, strong evidence from basic and clinical research indicates the involvement of a neurodegenerative component in the early stages of DR, which suggest the occurrence of these alterations before the clinical detection of vascular changes.[30–33] Thus, using an animal model enabled us to assess DR-related biological (molecular and cellular) alterations at (very) early, "silent" stages of the disease, which would be impossible to assess in humans with the diagnostic resources that are currently used in clinical practice, because they are not sensitive enough to detect such early biological alterations.

Because multiple molecular and cellular biological changes are occurring simultaneously in the diabetic retina, we cannot directly associate the changes in retinal texture to a specific biological alteration. However, biological changes in the retina as a whole may lead to changes in the structural arrangement of the retina, hence in retinal texture, which may then reflect aspects of the disease's pathophysiology and serve as an indicator of a pathogenic process. Accordingly, the present study hypothesizes that texture analysis may be a reliable method for detecting retinal changes at very early "silent" stages of DR.

Materials and Methods

Animal Model and Ethics

All procedures involving animals were conducted in accordance with the European Community directive guidelines (2010/63/EU) for the use of experimental animals, transposed to the Portuguese law in 2013 (Decreto-lei 113/2023), and were approved by the Animal Welfare Committee of the Coimbra Institute for Clinical and Biomedical Research (iCBR), Faculty of Medicine, University of Coimbra (ORBEA 02/2021), followed by the approval of the Direção Geral de Alimentação e Veterinária (DGAV – approval no. 0421/000/000/2021). Animal experimentation was also adhered according to the Association for Research in Vision and Ophthalmology (ARVO) Statement for the Use of Animals in Ophthalmic and Vision Research.

Male and female Wistar Han rats (Charles River Laboratories, Lyon, France), aged 10 weeks, were housed in certified facilities (2 animals per cage), with a temperature- and humidity-controlled environment, maintained under a 12-hour light/12-hour dark cycle, with ad libitum access to

Investigative Ophthalmology & Visual Science

water and food. Animals were randomly assigned to the control (Ctrl) and diabetic (T1D) groups. Type 1 diabetes was induced by an intraperitoneal (IP) injection of STZ (65 mg/kg in 10 mM sodium citrate buffer, pH 4.5) in fasting (6 hours) rats. Hyperglycemic status (glycaemia > 200 mg/dL) was confirmed 1 week later (Supplementary Fig. S1A). Information about the metabolic parameters monitored can be found in the Supplementary Materials.

OCT Data Acquisition

Retinas from the right eye of 44 control and 40 diabetic animals were imaged just before STZ injection (week 0) and 1, 2, and 4 weeks after diabetes onset (see the Supplementary Materials for details regarding the animal preparation). Retinal OCT volumes were acquired using the Micron IV OCT System (Phoenix Technology Group, Pleasanton, CA, USA), consisting of 512 B-scans each (composed of 512 A-scans of 1024 pixels in length), imaged at a predefined retinal region (horizontally aligned with the optic disc and vertically above it). B-scans were saved as non-compressed TIFF image files. The same operator performed all OCT data acquisitions. A large number of animals was used to obtain reliable results in the texture analysis. However, in the other experiments, retinal samples from the same animal were used to assess different parameters in order to minimize the number of animals used.

Automatic Retinal Segmentation

The segmentation of the retinal layers was achieved using a fully convolutional neural network, based on the ResNet architecture.[34,35] The network is composed of nine residual blocks organized in three stages (with 32, 64, and 128 filters, and strides of [2, 1], [2, 1], and [1, 1]). Each residual block contains three convolutional layers, each with ReLU activation and batch normalization. The skip-through connection bypasses the convolutional layers, enhancing the learning capacity by maintaining gradient flow. Additionally, max-pooling layers are incorporated to progressively reduce the spatial dimensions of the feature maps. A custom loss function was used, combining an accuracy measure and the mean absolute error. The accuracy component is calculated as the proportion of predictions within a specified threshold distance from the ground truth. The model was trained using the Adam optimizer with a learning rate of 0.001.

A total of six layers/layer-aggregate of the neuroretina were segmented: the retinal nerve fiber layer and ganglion cell layer complex (NFL-GCL), the inner plexiform layer (IPL), the inner nuclear layer (INL), the outer plexiform layer (OPL), the outer nuclear layer (ONL), and the inner/outer photoreceptor segments (IS/OS). The segmentation of the entire volume was achieved by combining the 512 segmented B-scans. The quality of the segmentation was evaluated by an expert (author S.O.) in a masked fashion.

Retinal Thickness

Retinal thickness maps were computed from the volumetric segmentation. The thickness of each retinal layer/conjugate, as well as the thickness of the entire retina, were calculated as the average distance between the respective segmented boundaries. Average thickness values per layer/conjugate and total retinal thickness were determined by averaging the 512 × 512 values, with one measurement per A-scan.

Texture Analysis

Projection mean-value fundus (MVF) images[17] were computed for each retinal layer. These are 2-dimensional (2D) images computed from volume OCT data, allowing us to project the 3D information of each layer onto a 2D plane, in which each pixel's value is the average of each A-scan values within the boundaries of the layer of interest, mimicking a fundus photograph taken at the layer of interest. After generating 20 × 20-pixel blocks cropped from the MVF images, the GLCM was applied. The GLCM is a popular method for texture-related feature extraction and is defined as a 2D histogram by which the probability of finding a transition from gray-level A to gray-level B along an established direction and an established distance (typically the next pixel, the distance of one pixel) is computed. How frequently the possible different transitions occur conveys information on the texture of the image being analyzed. In total, GLCM was computed for each of the 24 × 24 blocks per image, covering an area of 480 × 480 pixels centered on the projection images. A diagram showing the texture analysis workflow is provided in Supplementary Materials (Supplementary Fig. S2).

GLCM was computed at four direction angles (0, 45, 90, and 135 degrees) using a one-pixel scale considering symmetry (i.e. at 180 degrees apart, the angles are considered the same). For each resulting GLCM, 20 features were extracted (Supplementary Table S1), specifically: the inverse difference moment/energy, contrast/inertia, correlation, angular second moment/uniformity/homogeneity, sum average, sum of squares, sum variance, sum entropy, difference variance, difference entropy, information measure of correlation I (IMCI), information measure of correlation II (IMCII), and entropy were computed, as described by Haralick et al.[36]; autocorrelation and maximum probability, as described by Haralick et al.[37]; cluster prominence and cluster shade, as described by Conners et al.[38]; inverse difference normalized (INN) and inverse difference moment normalized (IDN), as described by Clausi et al.[39]; and dissimilarity, as described by Soh et al.[40]

Because distinct directions for the transitions between gray-level intensities can be used and texture metrics were computed in all possible directions, the maximum feature value across the four directions averaged for all the blocks was considered. This resulted in a total of 20 features per layer.

Electroretinography

Electroretinograms were recorded before STZ injection (week 0) and 1, 2, and 4 weeks after diabetes onset. The scotopic threshold response (STR) was first recorded by stimulating both eyes with a 0.000095 cd·s/m^2 light stimulus, followed by the stimulation with light flashes ranging from 0.0095 to 9.49 cd·s/m^2 to register the scotopic and photopic luminance responses. For the photopic flicker response, white light flashes (0.95, 3, and 9.49 cd·s/m^2) were delivered 10 times at 6.3 Hz. See the Supplementary Materials for details.

Immunofluorescence

Retinal Wholemounts. After euthanizing the animals by cervical dislocation while they were under anesthesia, the retinas were dissected and immunostained with claudin-5,

Table 1. List of Antibodies Used for Immunofluorescence of Retinal Wholemounts

Antibody	Dilution	Company	Catalog Number
Mouse anti-occludin	1:100	Invitrogen	33–1500
Rabbit anti-claudin-5	1:100	Invitrogen	34–1600
Rabbit anti-ZO-1	1:100	Invitrogen	40–2200
Alexa Fluor 488 Goat Anti-Rabbit	1:200	Invitrogen	A-11008
Alexa Fluor 568 Goat Anti-Mouse	1:200	Invitrogen	A-11004

Table 2. List of Antibodies Used for Immunofluorescence of Retinal Sections

Antibody	Dilution	Company	Catalog Number
Rabbit anti-Iba1	1:1,000	Wako	019-19741
Mouse anti-MHC class II (OX-6)	1:200	Bio-Rad	MCA46A647
Chicken anti-GFAP	1:500	Millipore	AB5541
Rabbit anti-vimentin	1:500	Abcam	ab92547
Alexa Fluor 488 goat anti-rabbit	1:200	Invitrogen	A-11008
Alexa Fluor 568 goat anti-chicken	1:200	Invitrogen	A-11041
Alexa Fluor 568 goat anti-mouse	1:200	Invitrogen	A-11004

Table 3. List of Antibodies Used for Western Blot

Antibody	Dilution	Company	Catalog Number
Rabbit anti-occludin	1:200	Invitrogen	71–1500
Rabbit anti-claudin-5	1:200	Invitrogen	34–1600
Rabbit anti-ZO-1	1:200	Invitrogen	40–2200
Rabbit anti-IL-1β	1:200	Abcam	ab9722
Rabbit anti-TNF	1:200	Abcam	ab66579
Goat anti-calnexin	1:1,000	Sicgen	AB0041-500
HRP goat anti-rabbit	1:10,000	Bio-Rad	1706515
HRP rabbit anti-goat	1:10,000	Invitrogen	61–1620

occludin, and zonula occludens-1 (ZO-1; Table 1). Detailed information on the immunofluorescence protocol and image analysis can be found in the Supplementary Material.

Retinal Cryosections. Retinal sections (14-µm thick) were immunostained with Iba1, OX-6/MHC II, glial fibrillary acidic protein (GFAP), and vimentin antibodies (Table 2), following the protocol and analysis described in the Supplementary Material.

Evans Blue Assay

Retinal vascular leakage was qualitatively assessed using the Evans blue dye, which binds irreversibly to serum albumin (see the Supplementary Material for information regarding the Evans blue methodology).

Western Blot

The expression levels of the proteins claudin-5, occludin, ZO-1, interleukin-1 beta (IL-1β), and tumor necrosis factor (TNF; Table 3) were assessed by Western blot in retinal homogenates. Detailed information is described in the Supplementary Material.

Enzyme-Linked Immunosorbent Assay

To prepare tissue homogenates, one retina from each eye was homogenized in lysis buffer (20 mM imidazole HCl, 100 mM KCl, 1 mM $MgCl_2$, 1% [vol./vol.] Triton X-100, 1 mM EGTA, 1 mM EDTA, 10 mM NaF, 1 mM Na_3VO_4 [activated] supplemented with complete miniprotease inhibitor cocktail tablets). Rat IL-1β and TNF enzyme-linked immunosorbent assay (ELISA) kits (#RAB0478 and #RAB0480; Sigma-Aldrich, St. Louis, MO, USA) were used to measure the levels of IL-1β and TNF in retinal homogenates, respectively, following the manufacturer's instruction (see the Supplementary Material for more details).

Statistical Analysis

Statistical analysis was performed using SPSS (version 27; IBM Corp., Armonk, NY, USA). The ANCOVA test was used to assess differences between groups for each individual time point of the study (weeks 1, 2, and 4) after adjusting for the baseline (week 0), which was used as a quantitative covariate. Additionally, repeated measures 2-way ANOVA was performed to test the effect of diabetes over time during the study period (the control group was also analyzed to check for any potential bias in the conclusions). Results from metabolic parameters, Western blot, and immunofluorescence were analyzed using unpaired Student's *t*-test, or by Mann-Whitney test in datasets that did not present a Gaussian distribution, which was assessed with Shapiro-Wilk normality test. We considered a statistical significance of 5%. All results are presented as mean ± SEM, except for the graphs of the retinal texture, in which the results are expressed by box plots showing the median (horizontal line), 25th and 75th percentiles (box), and minimum and maximum (error bars).

Results

Type 1 Diabetes Significantly Impacts Retinal Texture Early After Disease Onset

According to data previously published by members of our team, changes in retinal texture have been suggested as an early diagnosis biomarker for brain and eye disorders.[22,23] In this context, this study sought to identify retinal texture metrics for the early detection of DR, providing evidence for applying this methodology. Several GLCM-based texture parameters were significantly affected in diabetic rats, compared to the respective control animals.

Four weeks after diabetes onset, all retinal layers presented a decrease in autocorrelation (Fig. 1A(1–6)), correlation (Fig. 1B(1–6)), homogeneity (Fig. 1C(1–6)), IMCII (Fig. 1D(1–6)), IDN (Fig. 1E(1–6)), INN (Fig. 1F(1–6)), and sum average (Fig. 1G(1–6)). Similar effects in all retinal layers were observed for correlation, homogeneity, IMCII, IDN, and INN at week 2. Additionally, autocorrelation and sum average also showed a decrease at 2 weeks of diabetes in the INL (see Fig. 1A(3), 1G(3)), ONL (see Fig. 1A(5), 1G(5)), and IS/OS (see Fig. 1A(6), 1G(6)). One week after inducing diabetes, no changes were observed in most of the metrics assessed for almost all retinal layers, apart from a few exceptions. Indeed, ONL texture experienced an increase at week 1 in correlation, homogeneity, IMCII, IDN, and INN texture metrics (see Fig. 1B(5), 1C(5), 1D(5), 1E(5), 1F(5)). Although these early changes in retinal texture were subtle, they were statistically significant, suggesting that texture analysis has the potential to detect early retinal changes. The mean values ± SEM and the corresponding significance P values are provided in Supplementary Table S2.

Type 1 Diabetes Progression Enhances Changes in Texture

The impact of diabetes duration on texture parameters was also investigated (Table 4). Overall, the diabetic animals showed a weekly reduction in the texture metrics throughout the experimental period. Although no differences were found in any texture parameter from week 0 to week 1, significant changes were observed at week 2 compared with the earlier weeks (0 and/or 1), specifically in the texture metrics correlation, homogeneity, IMCII, IDN, and INN, in all retinal layers, with the exception for the NFL-GCL regarding the metrics correlation, IMCII, and IDN. Statistical differences in diabetic animals were also found at week 2 compared with weeks 0 and/or 1 in autocorrelation and sum average, but only in NFL-GCL and IS/OS retinal layers. Comparing week 4 to week 2, the autocorrelation and sum average texture metrics presented a decrease in the NFL-GCL, IPL, and OPL, whereas reductions in homogeneity, IDN, and INN were observed exclusively in the NFL-GCL. The mean values ± SEM are provided in Supplementary Table S3. To check for potential bias in the conclusions, a similar analysis of the time effect was also carried out on control animals; however, no consistent effects were observed (Supplementary Tables S4, S5).

Given the marked changes in retinal texture observed in diabetic animals, which became more significant with the duration of diabetes, we sought to evaluate structural, functional, molecular, and cellular changes associated with the pathophysiology of DR in order to determine whether changes in retinal texture might be concomitant with disease-related alterations, even if not directly attributed to texture itself.

Type 1 Diabetes Induces Retinal Thinning

OCT images were also used to assess the thickness of several retinal layers (NFL-GCL, IPL, INL, OPL, ONL, and IS/OS) as well as the total retinal thickness (Figs. 2A–H). Subtle retinal thinning was found in diabetic rats since the first week, specifically in IPL (2.59%, 2.80%, and 2.93% at weeks 1, 2, and 4, respectively, $P < 0.001$; see Fig. 2B), INL (3.81%, 4.21%, and 1.91% at weeks 1, 2, and 4, respectively, $P < 0.001$; see Fig. 2C), and IS/OS (2.91%, $P = 0.004$, 4.98%, $P < 0.001$, and 2.64%, $P = 0.004$ at weeks 1, 2, and 4, respectively; see Fig. 2F), compared to the control animals. Regarding the total retinal thickness (see Fig. 2G), a significant thinning was observed in diabetic rats at weeks 1, 2, and 4 (1.84%, 2.43%, and 1.58% decrease, respectively, $P < 0.001$), compared to aged-matched controls.

Type 1 Diabetes Affects Retinal Function Under Scotopic Conditions

The impact of diabetes on retinal physiological activity was assessed by ERG, a procedure that measures the electrical response to light flashes. In diabetic rats, the positive STR (pSTR) amplitude markedly decreased at weeks 2 and 4 (Ctrl; $N = 25$: 51.5 ± 5.8 µV and 48.9 ± 5.6 µV vs. T1D; $N = 25$: 32.1 ± 3.8 µV [$P = 0.023$] and 29.4 ± 3.1 µV [$P = 0.013$], respectively; Fig. 3A), whereas the negative STR (nSTR) amplitude was significantly reduced only at week 1 (Ctrl; $N = 25$: 70.3 ± 7.5 µV vs. T1D; $N = 25$: 39.9 ± 2.7 µV, $P = 0.038$; Fig. 3C). Moreover, STZ-induced diabetic rats displayed a significant delay in the a-wave response from the first week of diabetes onward (Figs. 3M–P), as reflected by increased area under the curve (AUC) values (Ctrl; $N = 25$: 111.2 ± 0.9, 112.5 ± 0.9, and 114.7 ± 1.0 vs. T1D; $N = 25$: 116.3 ± 1.2 [$P < 0.001$], 117.8 ± 1.6 [$P = 0.008$], and 122.0 ± 1.4 [$P < 0.001$] at weeks 1, 2, and 4, respectively; see Fig. 3P). The b-wave latency remained unchanged (Figs. 3Q–T).

Regarding the scotopic oscillatory potentials (OPs), increased latencies were noted in OP1 at weeks 1, 2, and 4 in response to 3 cd·s/m^2 (Ctrl; $N = 25$: 15.4 ± 0.2 ms, 15.5 ± 0.2 ms, and 15.7 ± 0.1 ms vs. T1D; $N = 25$: 16.0 ± 0.2 ms [$P = 0.014$], 16.3 ± 0.2 ms [$P = 0.004$], and 16.8 ± 0.2 ms [$P < 0.001$]; Fig. 4C) and 9.49 cd·s/m^2 light stimuli (Ctrl; $N = 25$: 14.9 ± 0.1 ms, 14.9 ± 0.1 ms, and 15.2 ± 0.2 ms vs. T1D; $N = 25$: 15.4 ± 0.2 ms [$P = 0.043$], 15.7 ± 0.2 ms [$P < 0.001$], and 15.9 ± 0.2 ms [$P = 0.006$], respectively; Fig. 4D). This delay was consistent in OP2, OP3, and OP4 from the first week of diabetes onward, under light stimuli of 3 cd·s/m^2 (Figs. 4G, 4K, 4O, respectively) and 9.49 cd·s/m^2 (Figs. 4H, 4L, 4P, respectively).

Type 1 Diabetes Induces Subtle Changes in the Tight Junction Proteins, Without Effect on the Blood-Retinal Barrier Permeability

To investigate the effect of diabetes on tight junction proteins, the immunoreactivity and the content of claudin-5, occludin, and ZO-1 proteins were evaluated in retinal wholemounts and homogenates by immunofluorescence and Western blot, respectively. In diabetic animals, compared to the respective controls, a qualitative analysis of the retinal wholemounts revealed a decrease in claudin-5 immunoreactivity in the deep capillary plexus (DCP) at weeks 2 and 4 (Fig. 5A) and in the smaller vessels of the superficial vascular plexus (SVP) at week 4 (Supplementary Fig. S4). Consistently, significantly lower claudin-5 protein levels were detected in total retinal extracts at week 4 (5.61% decrease; $P = 0.050$; Fig. 5E). Occludin immunoreactivity also decreased in the DCP of diabetic animals at week 4 (Fig. 5B), although no differences in its protein content were observed (Fig. 5F). Regarding ZO-1, diabetic animals showed a slight tendency toward a decrease in the SVP at week 4 (Fig. 5C), compared to the respective controls, without

Investigative Ophthalmology & Visual Science

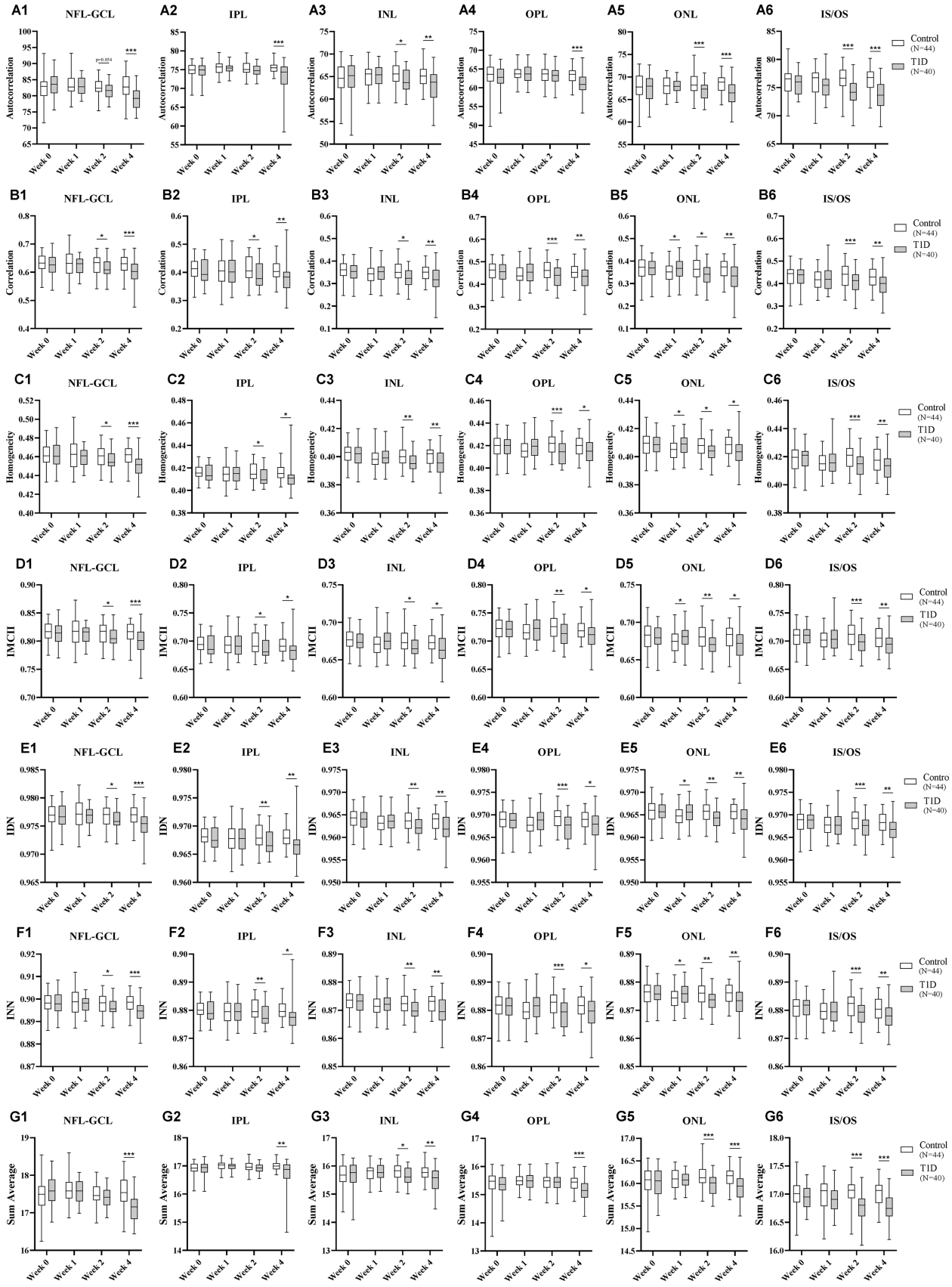

Figure 1. Early changes triggered by diabetes in retinal texture extracted from OCT retinal images. Diabetic Wistar rats (induced by 65 mg/kg STZ, IP; T1D group; $N = 40$), presented changes in several GLCM-based textural parameters extracted from OCT retinal images in all retinal layers, compared with age-matched controls (Ctrl group; $N = 44$), as follows: (**A1-A6**) autocorrelation; (**B1–B6**) correlation; (**C1–C6**) homogeneity; (**D1–D6**) information measure of correlation II (IMCII); (**E1–E6**) inverse difference moment normalized (IDN); (**F1–F6**) inverse

difference normalized (INN); (**G1–G6**) sum average. The results are expressed by box plots showing the median (*horizontal line*), 25th and 75th percentiles (*box*), and minimum and maximum (*error bars*) for each of the six defined retinal layers (NFL-GCL, retinal nerve fiber layer and ganglion cell layer complex; IPL, inner plexiform layer; INL, inner nuclear layer; OPL, outer plexiform layer; ONL, outer nuclear layer; and IS/OS, inner/outer photoreceptor segments) per texture parameter. Statistical analysis was performed using the ANCOVA test, considering the baseline values (week 0) as a quantitative covariate. $^{*}P \leq 0.05$, $^{**}P < 0.01$, $^{***}P < 0.001$, versus the age-matched Ctrl group. STZ, streptozotocin; GLCM, gray-level co-occurrence matrix; OCT, optical coherence tomography; T1D, type 1 diabetes.

any significant differences in the protein levels (Fig. 5G). Despite the minor diabetes-induced changes in tight junction proteins, no vessel leakage was detected by the Evans blue assay, after 4 weeks of diabetes, compared to the control animals (Fig. 5D), suggesting that the blood-retinal barrier function remained unaffected.

Type 1 Diabetes Early Increases the Cell Density of Iba1-Positive Cells in the Retina

Much evidence suggests the involvement of neuroinflammation in the pathogenesis of DR, with increased levels of proinflammatory cytokines,[28,41] along with the activation of glial cells.[42–44] In our type 1 diabetes animal model, 4 weeks of diabetes did not result in alterations in IL-1β protein levels (Figs. 6A, 6B), compared with age-matched controls, as assessed by Western blot and ELISA, respectively. Similarly, no changes were detected in the TNF protein content (Fig. 6C) in retinal homogenates by Western blot. TNF levels were also assessed by ELISA, but the protein could not be detected. Moreover, since the first week of diabetes, Iba1-positive cells (microglia/macrophages) significantly increased in retinal cryosections from diabetic animals, compared to age-matched controls (increase of 24.4%, $P = 0.002$, 28.9%, $P = 0.008$, and 25.6%, $P = 0.004$ at weeks 1, 2, and 4, respectively; Figs. 6D, 6F). No OX-6/MHC II-positive cells (reactive microglia/macrophages) were detected in the retinas of both experimental groups (data not shown). Similarly, no alterations were observed in the morphology and activation of Müller cells (as assessed by vimentin and GFAP immunoreactivity, respectively; Figs. 6E, 6G).

Discussion

Current public health guidelines in developed countries recommend screening patients with diabetes every 1 to 2 years, provided that blood glucose levels are under control and there are no clinical signals of DR.[45,46] Despite the advances in the clinical management of DR, particularly for the late stages, treatment success is still limited due to delayed disease diagnosis when compared to the diabetes onset, along with the lack of effective treatments specifically targeting the early stages of DR. Therefore, the discovery of novel diagnostic strategies targeting the very early detection of "silent" DR is of utmost importance.

In the present work, carried out using an animal model of STZ-induced type 1 diabetes, we evaluated the potential of texture analysis in assessing early changes in the retina. Accordingly, this study sought to provide evidence and proof of concept, as well as to lay the groundwork for developing a texture-based approach for the early diagnosis of DR before retinal changes can be detected with the diagnostic resources currently available in clinical practice (color fundus retinal photography, ultra-widefield color fundus retinal photography, fluorescein angiography, ultra-widefield fluorescein angiography, OCT, and angio-OCT). Additionally, we aimed to associate the changes in retinal texture with alterations typically linked to the pathophysiology of DR, such as structural (layer thickness) and functional (ERG) alterations, as well as molecular and cellular changes, including glial and vascular alterations. Hence, using an animal model of type 1 diabetes was crucial in this study, enabling us to assess retinal changes at very early, "silent" disease stages, as well as biological (molecular and cellular) parameters that cannot be assessed in vivo in humans, because the technology currently used in the clinical diagnosis of DR cannot detect those molecular and cellular alterations in the retina. Because patient data usually reflects stages in which DR is already diagnosed, it is critical to determine, before moving on with clinical studies, whether texture analysis can identify retinal texture changes when there is evidence of early and minor biological changes. Indeed, setting up a human study just to test a potential novel biomarker in the absence of any evidence linking retinal texture changes to diabetes-related molecular and cellular alterations in the retina seems unreasonable from an ethical and clinical point of view. Nevertheless, further studies using human OCT data are needed to verify the present findings.

Although OCT is mainly used to visualize the retinal structure and assess its thickness, different methods for analyzing OCT retinal images can be applied to extract more information about the retinal status. In previous studies conducted by some co-authors of this study, various approaches have been developed and have yielded promising results,[15,17,20] particularly in texture analysis of retinal OCT images.[22–25] In the present study, a similar texture-based methodology, adapted to the rat retina, was applied. Using this methodology for the first time in the context of diabetes, we were able to identify early differences between the diabetic and control animals in several retinal texture metrics (autocorrelation, correlation, homogeneity, IMCII, IDN, INN, and sum average), with all retinal layers being significantly affected. Moreover, the results obtained for the five most affected texture metrics (correlation, homogeneity, IMCII, IDN, and INN) were very consistent, meaning that retinal texture was affected in the same retinal layers at the same weeks after diabetes onset. Changes detected in autocorrelation and sum average were also consistent, although these were less pronounced compared with the other texture metrics. In addition to comparisons between experimental groups, the evaluation of the texture parameters over time allowed for an in-depth analysis into the retinal texture progression throughout the disease. Indeed, 7 texture metrics presented a weekly reduction in diabetic animals from week 1 to week 4, in almost all retinal layers. Considering these results, our methodology proved to be consistent in discriminating retinal texture between diabetic and control animals and detecting texture changes over the disease course.

The texture analysis approach applied in the present work conveys multivariate information on the spatial distribution of image intensity, providing information on subtle

Investigative Ophthalmology & Visual Science

Table 4. Statistical Evaluation of the Textural Parameters Extracted From Retinal OCT Images of Diabetic Animals Over the Course of the Disease

		Nerve Fiber Layer - Ganglion Cell Layer Complex			Inner Plexiform Layer			Inner Nuclear Layer			Outer Plexiform Layer			Outer Nuclear Layer			Inner/Outer Photoreceptors Segments		
		Sig. (2-Way RM ANOVA) (*P* Value)			Sig. (2-Way RM ANOVA) (*P* Value)			Sig. (2-Way RM ANOVA) (*P* Value)			Sig. (2-Way RM ANOVA) (*P* Value)			Sig. (2-Way RM ANOVA) (*P* Value)			Sig. (2-Way RM ANOVA) (*P* Value)		
GLCM-based Textural Parameters		**Week 1**	**Week 2**	**Week 4**	**Week 1**	**Week 2**	**Week 4**	**Week 1**	**Week 2**	**Week 4**	**Week 1**	**Week 2**	**Week 4**	**Week 1**	**Week 2**	**Week 4**	**Week 1**	**Week 2**	**Week 4**
Autocorrelation	Week 0	1.000	0.023[a]	0.000[a]	0.866	1.000	0.030[a]	1.000	1.000	0.025[a]	0.149	1.000	0.144	1.000	1.000	0.322	1.000	0.003[a]	0.001[a]
	Week 1		0.044[a]	0.000[a]		0.374	0.000[a]		0.076	0.000[a]		0.746	0.000[a]		0.071	0.005[a]		0.057	0.021[a]
	Week 2			0.002[a]			0.010[a]			0.057			0.000[a]			1.000			1.000
Correlation	Week 0	1.000	0.141	0.000[a]	1.000	0.081	0.003[a]	1.000	0.007[a]	0.000[a]	1.000	0.017[a]	0.005[a]	1.000	0.076	0.001[a]	1.000	0.003[a]	0.000[a]
	Week 1		0.188	0.001[a]		0.004[a]	0.003[a]		0.002[a]	0.000[a]		0.009[a]	0.003[a]		0.045[a]	0.001[a]		0.122	0.012[a]
	Week 2			0.179			0.556			0.410			1.000			0.321			1.000
Homogeneity	Week 0	1.000	0.012[a]	0.000[a]	1.000	0.042[a]	0.026[a]	1.000	0.001[a]	0.001[a]	1.000	0.030[a]	0.127	1.000	0.030[a]	0.003[a]	0.978	0.001[a]	0.001[a]
	Week 1		0.044[a]	0.000[a]		0.004[a]	0.030[a]		0.004[a]	0.014[a]		0.007[a]	0.036[a]		0.039[a]	0.003[a]		0.099	0.052
	Week 2			0.047[a]			1.000			1.000			1.000			1.000			1.000
Information measure of correlation II	Week 0	1.000	0.115	0.000[a]	1.000	0.249	0.018[a]	1.000	0.035[a]	0.003[a]	1.000	0.028[a]	0.005[a]	1.000	0.079	0.008[a]	1.000	0.004[a]	0.000[a]
	Week 1		0.137	0.000[a]		0.006[a]	0.007[a]		0.003[a]	0.001[a]		0.007[a]	0.002[a]		0.033[a]	0.003[a]		0.077	0.008[a]
	Week 2			0.158			0.954			1.000			1.000			1.000			1.000
Inverse difference moment normalized	Week 0	1.000	0.091	0.000[a]	1.000	0.032[a]	0.005[a]	1.000	0.001[a]	0.000[a]	1.000	0.032[a]	0.070	1.000	0.042[a]	0.001[a]	1.000	0.001[a]	0.001[a]
	Week 1		0.074	0.000[a]		0.002[a]	0.006[a]		0.004[a]	0.003[a]		0.009[a]	0.024[a]		0.045[a]	0.001[a]		0.142	0.039[a]
	Week 2			0.046[a]			1.000			1.000			1.000			0.510			1.000
Inverse difference normalized	Week 0	1.000	0.033[a]	0.000[a]	1.000	0.032[a]	0.010[a]	1.000	0.001[a]	0.000[a]	1.000	0.031[a]	0.088	1.000	0.036[a]	0.001[a]	0.983	0.001[a]	0.001[a]
	Week 1		0.055	0.000[a]		0.002[a]	0.012[a]		0.004[a]	0.005[a]		0.009[a]	0.029[a]		0.044[a]	0.002[a]		0.125	0.042[a]
	Week 2			0.043[a]			1.000			1.000			1.000			0.743			1.000
Sum average	Week 0	1.000	0.041[a]	0.000[a]	0.935	1.000	0.075	1.000	1.000	0.054	0.131	1.000	0.351	1.000	1.000	0.940	1.000	0.010[a]	0.004[a]
	Week 1		0.049[a]	0.000[a]		0.909	0.000[a]		0.131	0.000[a]		1.000	0.000[a]		0.120	0.011[a]		0.091	0.046[a]
	Week 2			0.001[a]			0.016[a]			0.051			0.000[a]			1.000			1.000

Summary of the results obtained from two-way repeated measures ANOVA test applied to the GLCM-based textural parameters extracted from OCT retinal images of diabetic Wistar rats (induced by STZ; 65 mg/kg, IP; T1D group; $N = 40$) for each retinal layer.

GLCM, gray-level co-occurrence matrix; OCT, optical coherence tomography; STZ, streptozotocin; T1D, type 1 diabetes.

[a] Significant decrease in the week indicated in the columns, compared to the corresponding week indicated in each row.

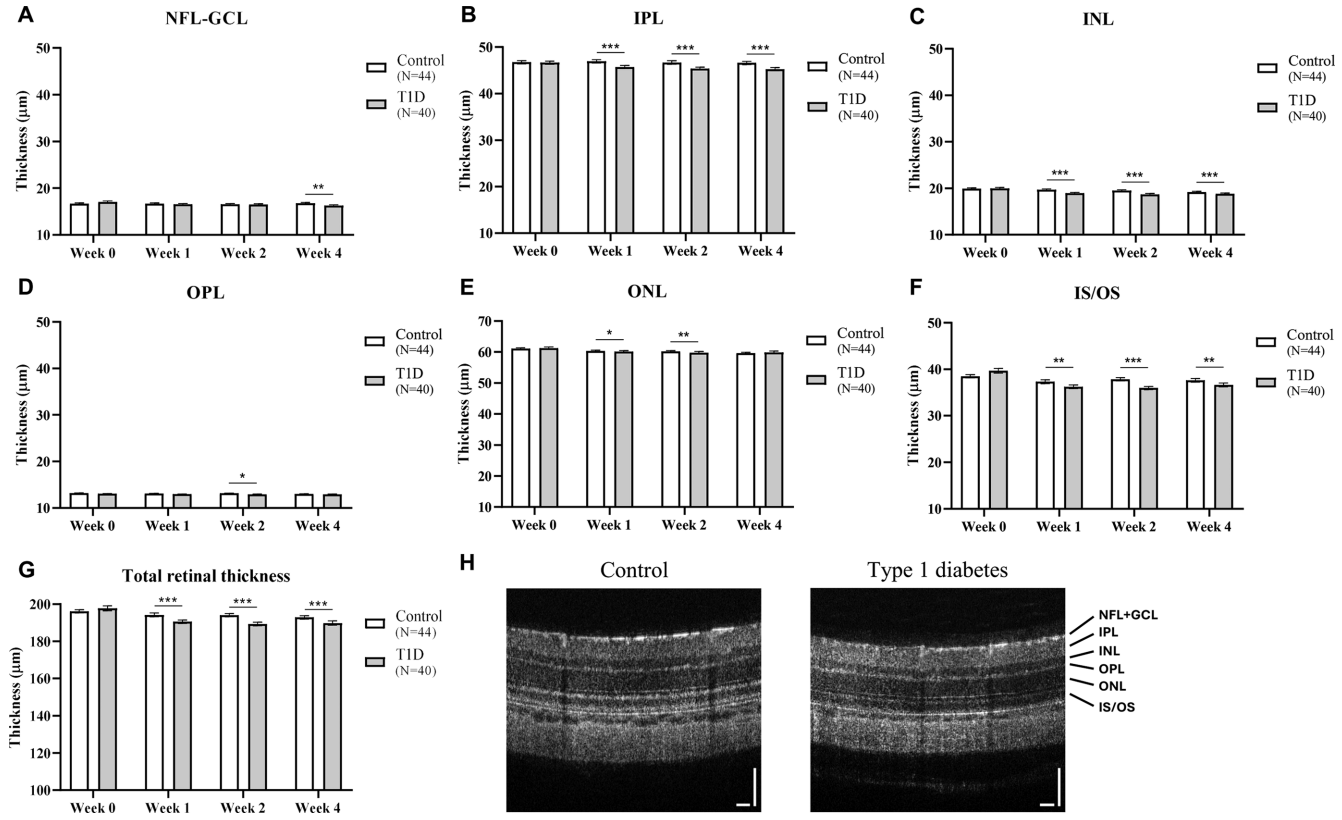

Figure 2. Impact of diabetes on retinal thickness. Diabetes (induced by STZ; 65 mg/kg, IP; T1D group; $N = 40$) induced retinal thinning in Wistar rats compared to the age-matched controls (Ctrl group; $N = 44$). The retinal thickness of control and diabetic rats was assessed in the following retinal layers: (**A**) retinal nerve fiber layer and ganglion cell layer complex (NFL-GCL); (**B**) inner plexiform layer (IPL); (**C**) inner nuclear layer (INL); (**D**) outer plexiform layer (OPL); (**E**) outer nuclear layer (ONL); (**F**) inner/outer photoreceptor segments (IS/OS). (**G**) Total retinal thickness was calculated as the sum of the six retinal layers. (**H**) Representative OCT images for Ctrl and T1D groups at week 4. Scale bar = 100 µm. Results are presented as mean ± SEM. Statistical analysis was performed using the ANCOVA test, considering the baseline values (week 0) as a quantitative covariate. $^{*}P \leq 0.05$, $^{**}P < 0.01$, $^{***}P < 0.001$, versus the aged-matched Ctrl group. STZ, streptozotocin; T1D, type 1 diabetes.

structural differences of the distinct retinal layers. Texture analysis allows expressing subtle changes in the retina well before these can be capture by thickness, which may explain the methodological performance achieved in this study. Although retinal thickness measurements detected subtle retinal thinning since the first week of diabetes, particularly in the inner plexiform and nuclear layers and in the photoreceptor segments, the remaining retinal layers showed more discrepant results, compared to retinal texture data. Because the retinal thickness measurements are not disease-specific and several eye conditions can have an impact on retinal thickness, the use of thickness-based methodologies in clinical practice is limited, particularly in the early stages of the disease. Nevertheless, assessing retinal thickness is undoubtedly indispensable in eye care currently. In the future, combined with other methodologies, such as texture analysis, it could provide the required tools for an early and accurate diagnosis of DR.

Recognizing DR as a neurovascular and a low-grade chronic neuroinflammatory disease,[2,5,47,48] we assessed several parameters related to potential physiological, molecular, and cellular changes associated with neuronal, glial, and vascular retinal cells, as well as changes related to neuroinflammation. This helped us understand whether the changes detected in retinal texture in several retinal layers could be concomitant with functional and biological retinal changes. Regarding retinal physiology, our results showed delayed implicit times under scotopic conditions in diabetic animals, which is in accordance with clinical[49,50] and preclinical[51–53] studies performed in early-stage DR. In addition, diabetic rats also exhibited compromised responses driven by the RGCs and cones, although these changes were subtler. In sum, ERG results indicate that diabetic retinas develop impaired retinal function from very early stages upon diabetes onset, which can eventually also support the early alterations found in the texture metrics.

Previous studies from our group reported that type 1 diabetes induces changes in retinal vascular permeability, which was appointed to be partially promoted by alterations in tight junction proteins along with an exacerbation of inflammatory and oxidative processes.[28,29,54,55] Similar effects were found in the current study, as evidenced by subtle changes in the tight junction proteins immunoreactivity, which did not induce any physiologically relevant effect on the blood-retinal barrier, and markers related to the immune response, namely increased Iba1-positive cells (microglia/macrophages). These results highlight the assumption of an early and low-grade retinal injury, which might somehow be reflected in the texture analysis.

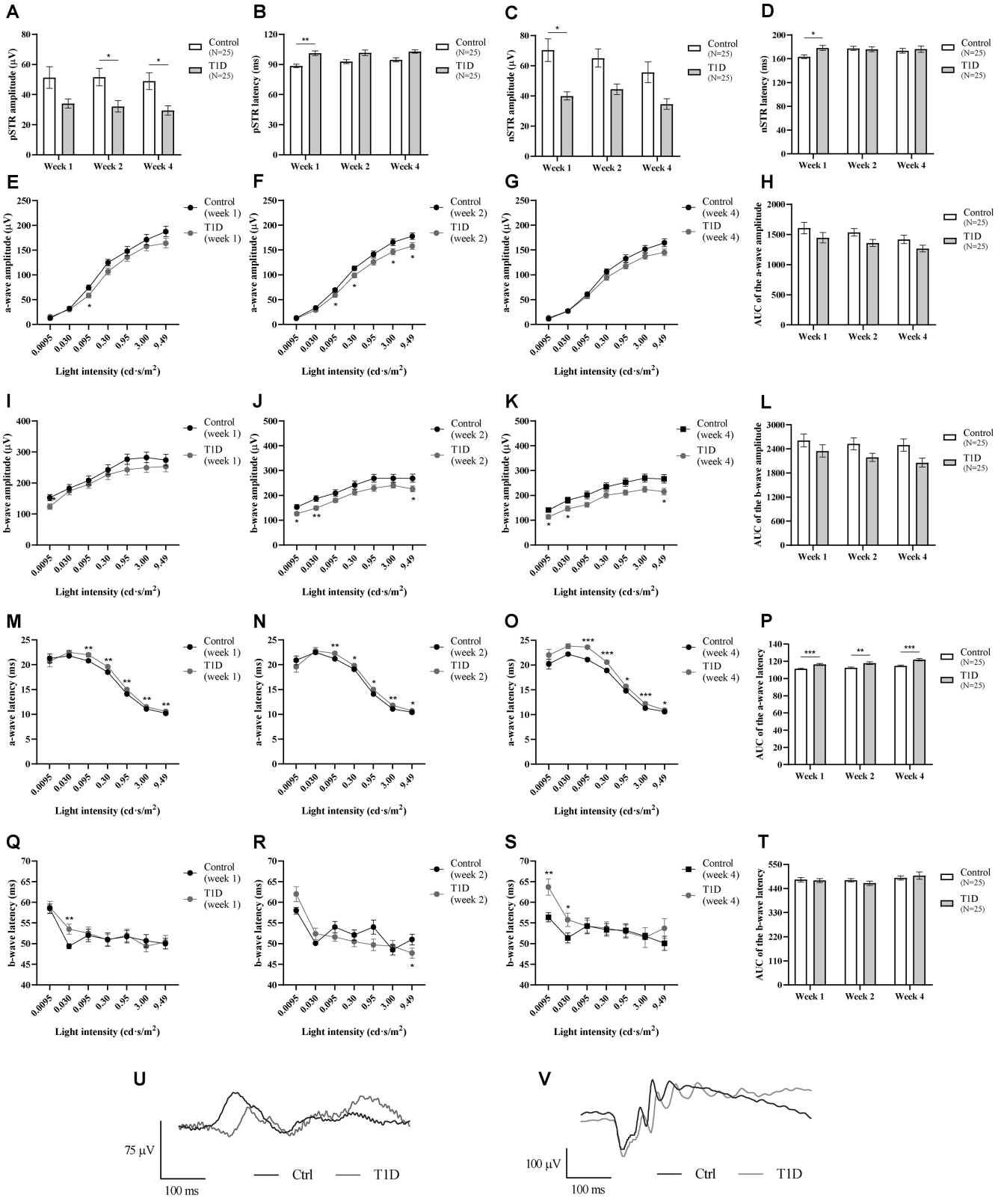

Figure 3. Impact of diabetes on retinal physiology. Scotopic retinal function was affected in diabetic Wistar rats (induced by STZ; 65 mg/kg, IP; T1D group; $N = 25$) early after diabetes onset, compared to the age-matched controls (Ctrl group; $N = 25$). The pSTR and nSTR (**A, C**) amplitudes and (**B, D**) latencies in response to a 0.000095 cd·s/m^2 light stimulus. Scotopic a-wave and b-wave amplitudes in response to 0.0095 to 9.49 cd·s/m^2 light stimuli recorded at (**E, I**) week 1, (**F, J**) week 2, and (**G, K**) week 4. Scotopic a-wave and b-wave latencies in response to 0.0095 to 9.45 cd·s/m^2 light stimuli recorded at (**M, Q**) week 1, (**N, R**) week 2, and (**O, S**) week 4. Area under the curve (AUC) of scotopic a-wave and b-wave (**H, L**) amplitudes and (**P, T**) latencies. Representative traces of (**U**) STR and (**V**) scotopic waves of control and diabetic animals recorded at week 4. Results are presented as mean ± SEM. Statistical analysis was performed using the ANCOVA test, considering the baseline values (week 0) as a quantitative covariate. *$P \leq 0.05$, **$P < 0.01$, ***$P < 0.001$, versus the aged-matched Ctrl group. STZ, streptozotocin; T1D, type 1 diabetes.

Investigative Ophthalmology & Visual Science

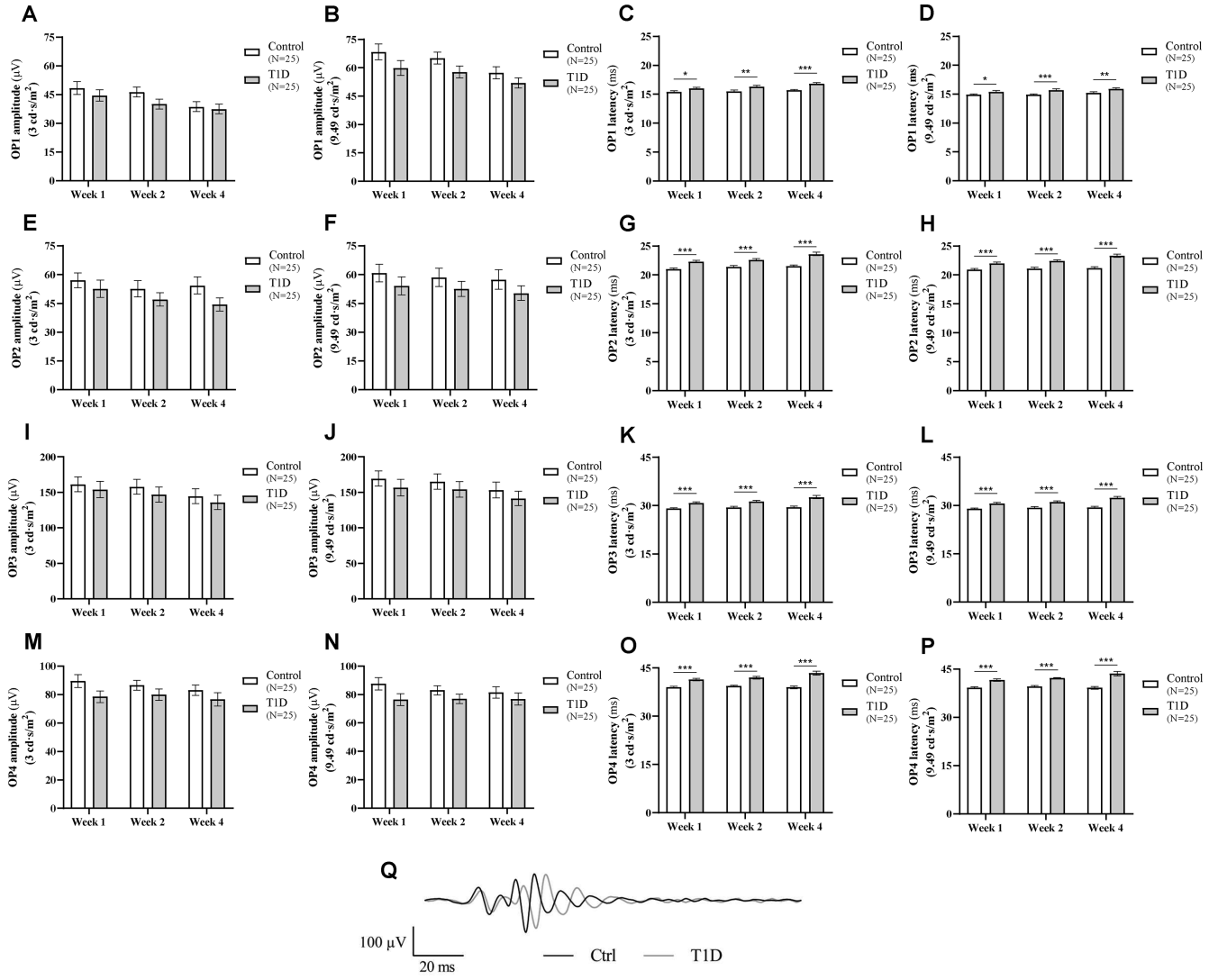

Figure 4. Diabetes affects OPs. Diabetes (induced by STZ; 65 mg/kg, IP; T1D group; $N = 25$) induced a marked delay in the scotopic OPs in Wistar rats compared to the age-matched controls (Ctrl group; $N = 25$). OP1, OP2, OP3, and OP4 amplitudes recorded in response to (**A**, **E**, **I**, and **M**, respectively) 3 cd·s/m^2 and (**B**, **F**, **J**, and **N**, respectively) 9.49 cd·s/m^2 light stimuli. Latencies of OP1, OP2, OP3, and OP4 recorded in response to (**C**, **G**, **K**, and **O**, respectively) 3 cd·s/m^2 and (**D**, **H**, **L**, and **P**, respectively) 9.49 cd·s/m^2 light stimuli. (**Q**) Representative traces of OPs of control and diabetic animals recorded at week 4 after applying an OFF-line digital filter (low frequency cutoff of 60 Hz). Results are presented as mean ± SEM. Statistical analysis was performed using the ANCOVA test, considering the baseline values (week 0) as a quantitative covariate. *$P \leq 0.05$, **$P < 0.01$, ***$P < 0.001$, versus the aged-matched Ctrl group. OP, oscillatory potential; STZ, streptozotocin; T1D, type 1 diabetes.

Based on these findings, our texture-based methodology, applied for the first time in the context of diabetes/DR, conveys distinct information on the impact of diabetes on the retina, very early after diabetes onset. Because we cannot directly associate changes in retinal texture to a specific molecular or cellular alteration, our approach would not fully match the definition of a biomarker outlined by the National Institutes of Health Biomarkers Definitions Working Group. Nevertheless, the multiple molecular and cellular biological alterations that occur in the diabetic retina may lead to changes in the structural arrangement of the retina, hence in retinal texture, that may then reflect aspects of the disease pathophysiology. Moreover, focusing only on indicators/biomarkers with a direct relation to a particular retinal biological process limits the opportunity to implement more innovative and powerful methods, such as texture analysis, thereby hampering scientific progress.

The molecular and cellular alterations in the retina described here cannot be assessed with the diagnostic resources currently available in ophthalmological practice, contributing to delayed diagnosis of DR. By combining several of the texture features, it was possible to extract patterns of significant differences between the diabetic and control groups, with very significant and consistent texture changes spreading across all six layers of the diabetic neuroretina. In contrast, the structural, functional, cellular, and molecular results were not always coherent throughout the study, with subtle differences, which further underlies the potential value of texture-based approaches. In conclu-

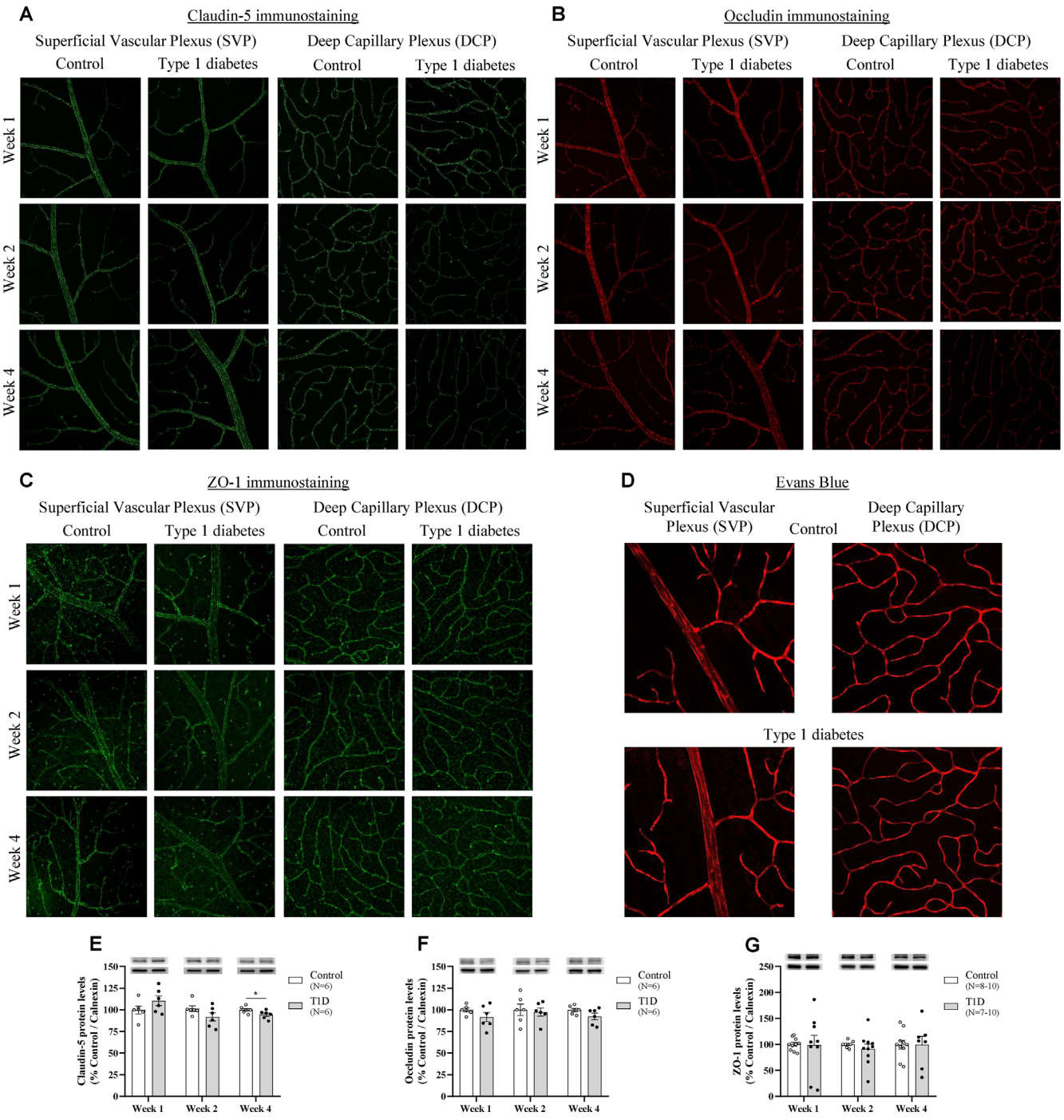

Figure 5. Diabetes induces subtle changes in tight junction proteins immunoreactivity, although without alterations in retinal vascular permeability. Diabetic Wistar rats (induced by STZ; 65 mg/kg, IP; T1D group) presented a decrease in claudin-5 and occludin immunostaining and a slight tendency to a decrease in ZO-1 immunostaining, assessed in retinal wholemounts, along with decreased protein levels of claudin-5 in retinal extracts, assessed by Western blot, compared to the age-matched controls (Ctrl group). Retinal vascular permeability was assessed by the Evans blue assay, but no vascular leakage was detected in diabetic animals. Representative images of retinal wholemounts immunostained for (**A**) claudin-5, (**B**) occludin, and (**C**) ZO-1. (**D**) Representative images showing Evans blue fluorescence in the retina. (**E**) Claudin-5, (**F**) occludin, and (**G**) ZO-1 protein levels assessed by Western blot, normalized to the loading control (calnexin), and expressed as percentage of the respective control. Representative images of protein immunoreactive bands are presented above the graphs, with the respective loading control (calnexin). Data are presented as mean ± SEM. Statistical analysis was performed using the unpaired Student's *t*-test. *$P \leq 0.05$, versus the aged-matched Ctrl group. STZ, streptozotocin; T1D, type 1 diabetes; ZO-1, zonula occludens-1.

sion, our study highlights the potential of texture analysis to provide powerful quantitative information on the retinal status, allowing us to spot differences under diabetic conditions. In order to implement this texture-based strategy in humans, an extensive clinical study is mandatory to properly identify and accurately validate which texture metrics best

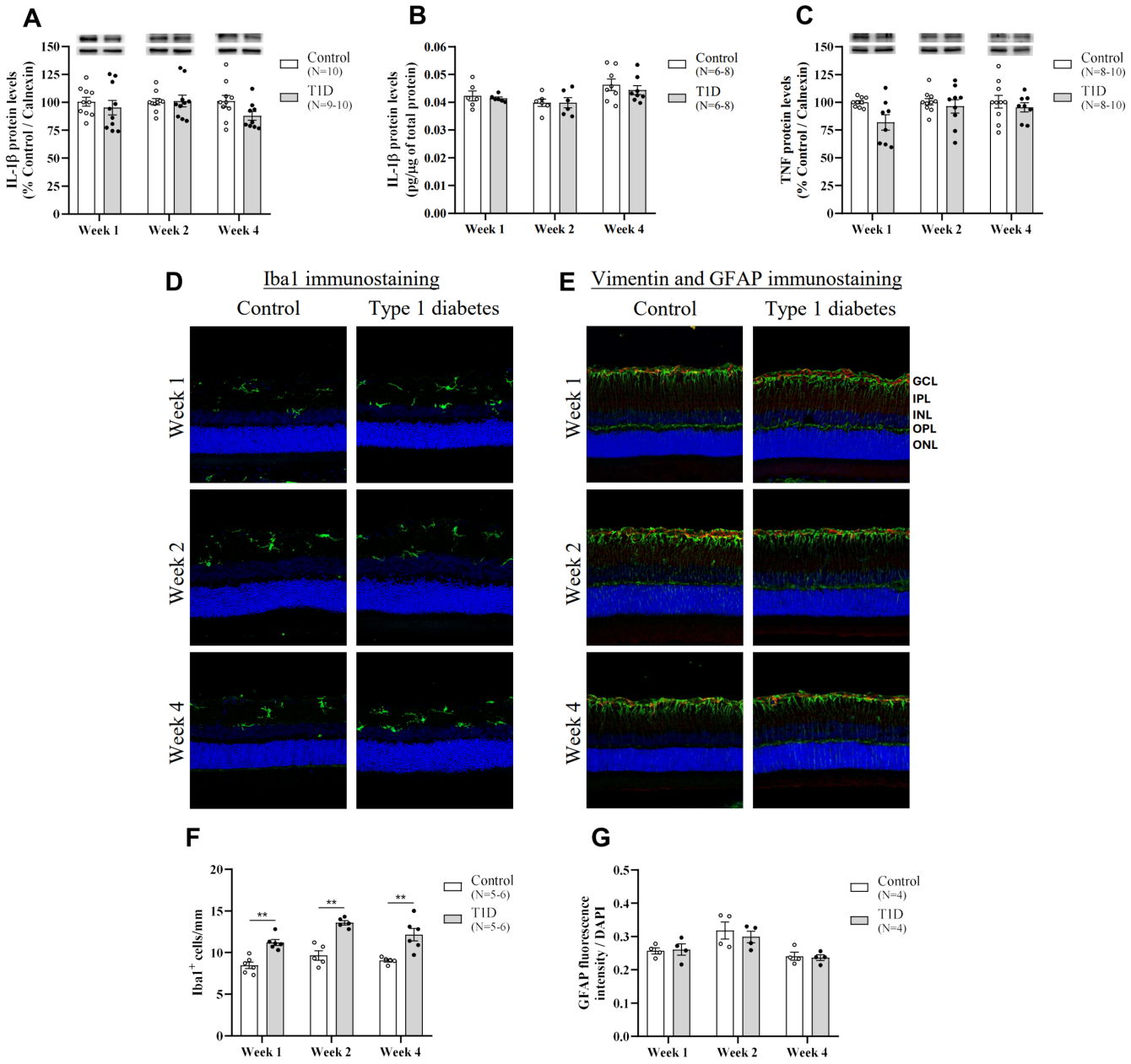

Figure 6. Diabetes triggers an increase in the number of Iba1-positive cells (microglia/macrophages) in the retina. Retinas from diabetic Wistar rats (induced by STZ; 65 mg/kg, IP; T1D group) presented an increased Iba1-positive cells density, compared to the age-matched controls (Ctrl group). Müller glial cell reactivity and the protein levels of pro-inflammatory cytokines remained unchanged. (**A**) IL-1β and (**C**) TNF protein levels were assessed by Western blot, normalized to the loading control (calnexin), and expressed as a percentage of the respective control. Representative images of protein immunoreactive bands are presented above the graphs, with the respective loading control (calnexin). (**B**) IL-1β protein levels assessed by ELISA. Representative images of retinal cryosections immunoassayed for (**D**) Iba1 and (**E**) vimentin and GFAP. The quantification of Iba1-positive cell counting (microglia/macrophages) and GFAP immunolabeling are presented below (**F** and **G**, respectively). Data are presented as mean ± SEM. Statistical analysis was performed using the unpaired Student's *t*-test, or by Mann-Whitney test in datasets that did not present a Gaussian distribution. $^{**}P < 0.01$, versus the aged-matched Ctrl group. GFAP, glial fibrillary acidic protein; IL-1β, interleukin-1 beta; STZ, streptozotocin; T1D, type 1 diabetes; TNF, tumor necrosis factor.

fit an effective biomarker for early DR. As a result, this study does not replace a clinical study, but it is crucial to provide evidence for the potential of texture analysis in identifying retinal alterations when early diabetes-related biological changes that would not be clinically detectable are occurring in the retina. Further work on this subject in other diabetic animal models, and particularly in humans, might enhance the discriminative capability of OCT image analysis, thereby helping to diagnose subclinical disease stages, in order to provide a closer follow-up of patients with early-grade DR.

Acknowledgments

The authors thank Francisco Caramelo from the Coimbra Institute for Clinical and Biomedical Research (iCBR), Area of

Environment Genetics and Oncobiology (CIMAGO), Faculty of Medicine, University of Coimbra, and from the Laboratory of Biostatistics and Medical Informatics (LBIM), Faculty of Medicine, University of Coimbra, for his support and guidance in the statistical analysis.

Supported by Foundation for Science and Technology, Portugal: 2020.07432.BD, PEst UIDB/04539/Base/2020 and UIDP/04539/Programatico/2020, and PEst UIDB/04950/Base/2020 and UIDP/04950/Programatico/2020. This study was also supported by Sociedade Portuguesa de Diabetologia (SPD), Portugal: Bolsa Charneco da Costa - Investigação Fundamental em Diabetologia, Bolsas e Prémios SPD 2024.

Disclosure: **S. Oliveira**, None; **P. Guimarães**, None; **E.J. Campos**, None; **R. Fernandes**, None; **J. Martins**, None; **M. Castelo-Branco**, None; **P. Serranho**, None; **P. Matafome**, None; **R. Bernardes**, None; **A.F. Ambrósio**, None

References

1. Kropp M, Golubnitschaja O, Mazurakova A, et al. Diabetic retinopathy as the leading cause of blindness and early predictor of cascading complications-risks and mitigation. *EPMA J*. 2023;14(1):21–42.
2. Duh EJ, Sun JK, Stitt AW. Diabetic retinopathy: current understanding, mechanisms, and treatment strategies. *JCI Insight*. 2017;2(14):e93751.
3. Sinclair SH, Schwartz SS. Diabetic retinopathy-an underdiagnosed and undertreated inflammatory, neuro-vascular complication of diabetes. *Front Endocrinol (Lausanne)*. 2019;10:843.
4. Rübsam A, Parikh S, Fort PE. Role of inflammation in diabetic retinopathy. *Int J Mol Sci*. 2018;19(4):942.
5. Bianco L, Arrigo A, Aragona E, et al. Neuroinflammation and neurodegeneration in diabetic retinopathy. *Front Aging Neurosci*. 2022;14:937999.
6. Jang HN, Moon MK, Koo BK. Prevalence of diabetic retinopathy in undiagnosed diabetic patients: a nationwide population-based study. *Diabetes Metab J*. 2022;46(4):620–629.
7. Popescu DP, Choo-Smith L-P, Flueraru C, et al. Optical coherence tomography: fundamental principles, instrumental designs and biomedical applications. *Biophys Rev*. 2011;3(3):155.
8. Fujimoto JG. Optical coherence tomography for ultrahigh resolution in vivo imaging. *Nat Biotechnol*. 2003;21(11):1361–1367.
9. Ruggeri M, Tsechpenakis G, Jiao S, et al. Retinal tumor imaging and volume quantification in mouse model using spectral-domain optical coherence tomography. *Opt Express*. 2009;17(5):4074–4083.
10. Venhuizen FG, van Ginneken B, van Asten F, et al. Automated staging of age-related macular degeneration using optical coherence tomography. *Invest Ophthalmol Vis Sci*. 2017;58(4):2318–2328.
11. Chen S-C, Chiu H-W, Chen C-C, Woung L-C, Lo C-M. A novel machine learning algorithm to automatically predict visual outcomes in intravitreal ranibizumab-treated patients with diabetic macular edema. *J Clin Med*. 2018;7(12):475.
12. De Fauw J, Ledsam JR, Romera-Paredes B, et al. Clinically applicable deep learning for diagnosis and referral in retinal disease. *Nat Med*. 2018;24(9):1342–1350.
13. Yazdanpanah A, Hamarneh G, Smith BR, Sarunic M V. Segmentation of intra-retinal layers from optical coherence tomography images using an active contour approach. *IEEE Trans Med Imaging*. 2011;30(2):484–496.
14. Seebock P, Waldstein SM, Klimscha S, et al. Unsupervised identification of disease marker candidates in retinal OCT imaging data. *IEEE Trans Med Imaging*. 2019;38(4):1037–1047.
15. Bernardes R, Santos T, Serranho P, Lobo C, Cunha-Vaz J. Noninvasive evaluation of retinal leakage using optical coherence tomography. *Ophthalmologica*. 2011;226(2):29–36.
16. Guimarães P, Rodrigues P, Celorico D, Serranho P, Bernardes R. Three-dimensional segmentation and reconstruction of the retinal vasculature from spectral-domain optical coherence tomography. *J Biomed Opt*. 2015;20(1):16006.
17. Guimarães P, Rodrigues P, Lobo C, et al. Ocular fundus reference images from optical coherence tomography. *Comput Med Imaging Graph*. 2014;38(5):381–389.
18. Ferreira H, Martins J, Moreira PI, et al. Longitudinal normative OCT retinal thickness data for wild-type mice, and characterization of changes in the 3×Tg-AD mice model of Alzheimer's disease. *Aging (Albany NY)*. 2021;13(7):9433–9454.
19. Bernardes R. Optical coherence tomography: health information embedded on OCT signal statistics. *Annu Int Conf IEEE Eng Med Biol Soc*. 2011;2011:6131–6133.
20. Rodrigues P, Guimarães P, Santos T, et al. Two-dimensional segmentation of the retinal vascular network from optical coherence tomography. *J Biomed Opt*. 2013;18(12):126011.
21. Santos M, Araujo A, Barbeiro S, et al. Simulation of cellular changes on optical coherence tomography of human retina. *Annu Int Conf IEEE Eng Med Biol Soc*. 2015;2015:8147–8150.
22. Ferreira H, Martins J, Nunes A, et al. Characterization of the retinal changes of the 3×Tg-AD mouse model of Alzheimer's disease. *Health Technol (Berl)*. 2020;10(4):875–883.
23. Nunes A, Silva G, Duque C, et al. Retinal texture biomarkers may help to discriminate between Alzheimer's, Parkinson's, and healthy controls. *PLoS One*. 2019;14(6):e0218826.
24. Nunes A, Ambrosio AF, Castelo-Branco M, Bernardes R. [Regular Paper] Texture biomarkers of Alzheimer's disease and disease progression in the mouse retina. In: *2018 IEEE 18th International Conference on Bioinformatics and Bioengineering (BIBE)*. 2018:41–46.
25. Bernardes R, Silva G, Chiquita S, Serranho P, Ambrósio AF. Retinal biomarkers of Alzheimer's disease: insights from transgenic mouse models. *Lect Notes Comput Sci (including Subser Lect Notes Artif Intell Lect Notes Bioinformatics)*. 2017;10317 LNCS:541–550.
26. Cai X, McGinnis JF. Diabetic retinopathy: animal models, therapies, and perspectives. *J Diabetes Res*. 2016;2016(1):3789217.
27. Olivares AM, Althoff K, Chen GF, et al. Animal models of diabetic retinopathy. *Curr Diab Rep*. 2017;17(10):93.
28. Gonçalves A, Marques C, Leal E, et al. Dipeptidyl peptidase-IV inhibition prevents blood-retinal barrier breakdown, inflammation and neuronal cell death in the retina of type 1 diabetic rats. *Biochim Biophys Acta*. 2014;1842(9):1454–1463.
29. Leal EC, Manivannan A, Hosoya KI, et al. Inducible nitric oxide synthase isoform is a key mediator of leukostasis and blood-retinal barrier breakdown in diabetic retinopathy. *Invest Ophthalmol Vis Sci*. 2007;48(11):5257–5265.
30. Antonetti DA, Silva PS, Stitt AW. Current understanding of the molecular and cellular pathology of diabetic retinopathy. *Nat Rev Endocrinol*. 2021;17(4):195–206.
31. Barber AJ, Lieth E, Khin SA, Antonetti DA, Buchanan AG, Gardner TW. Neural apoptosis in the retina during experimental and human diabetes. Early onset and effect of insulin. *J Clin Invest*. 1998;102(4):783–791.
32. Sohn EH, van Dijk HW, Jiao C, et al. Retinal neurodegeneration may precede microvascular changes characteristic of

diabetic retinopathy in diabetes mellitus. *Proc Natl Acad Sci USA*. 2016;113(19):E2655–E2664.

33. Martin PM, Roon P, Van Ells TK, Ganapathy V, Smith SB. Death of retinal neurons in streptozotocin-induced diabetic mice. *Invest Ophthalmol Vis Sci*. 2004;45(9):3330–3336.
34. Batista A, Guimarães P, Martins J, et al. Normative mice retinal thickness: 16-month longitudinal characterization of wild-type mice and changes in a model of Alzheimer's disease. *Front Aging Neurosci*. 2023;15:1161847.
35. Batista A, Guimarães P, Serranho P, et al. Retinal imaging in animal models: searching for biomarkers of neurodegeneration. *Front Ophthalmol*. 2023;3:1156605.
36. Haralick RM, Shanmugam K, Dinstein I. Textural features for image classification. *IEEE Trans Syst Man Cybern*. 1973;SMC-3(6):610–621.
37. Haralick RM. Statistical and structural approaches to texture. *Proc IEEE*. 1979;67(5):786–804.
38. Conners RW, Trivedi MM, Harlow CA. Segmentation of a high-resolution urban scene using texture operators. *Comput Vision, Graph Image Process*. 1984;25(3):273–310.
39. Clausi DA. An analysis of co-occurrence texture statistics as a function of grey level quantization. *Can J Remote Sens*. 2002;28(1):45–62.
40. Soh L-K, Tsatsoulis C. Texture analysis of SAR sea ice imagery using gray level co-occurrence matrices. *IEEE Trans Geosci Remote Sens*. 1999;37(2):780–795.
41. Demircan N, Safran BG, Soylu M, Ozcan AA, Sizmaz S. Determination of vitreous interleukin-1 (IL-1) and tumour necrosis factor (TNF) levels in proliferative diabetic retinopathy. *Eye (Lond)*. 2006;20(12):1366–1369.
42. Mizutani M, Gerhardinger C, Lorenzi M. Müller cell changes in human diabetic retinopathy. *Diabetes*. 1998;47(3):445–449.
43. Campos A, Campos EJ, Martins J, Rodrigues FSC, Silva R, Ambrósio AF. Inflammatory cells proliferate in the choroid and retina without choroidal thickness change in early type 1 diabetes. *Exp Eye Res*. 2020;199:108195.
44. Campos A, Martins J, Campos EJ, Silva R, Ambrósio AF. Choroidal and retinal structural, cellular and vascular changes in a rat model of type 2 diabetes. *Biomed Pharmacother*. 2020;132:110811.
45. World Health Organization. Diabetic Retinopathy Screening: A Short Guide. Vol. 53. 2020. Available at: https://iris.who.int/bitstream/handle/10665/336660/9789289055321-eng.pdf.
46. American Diabetes Association Professional Practice Committee. 12. Retinopathy, neuropathy, and foot care: standards of care in diabetes—2024. *Diabetes Care*. 2023;47(Supplement_1):S231–S243.
47. Santiago AR, Boia R, Aires ID, Ambrósio AF, Fernandes R. Sweet stress: coping with vascular dysfunction in diabetic retinopathy. *Front Physiol*. 2018;9:820.
48. Cunha-Vaz JG. Pathophysiology of diabetic retinopathy. *Br J Ophthalmol*. 1978;62(6):351–355.
49. Luu CD, Szental JA, Lee S-Y, Lavanya R, Wong TY. Correlation between retinal oscillatory potentials and retinal vascular caliber in type 2 diabetes. *Invest Ophthalmol Vis Sci*. 2010;51(1):482–486.
50. Tănasie CA, Dan AO, Ică OM, et al. Retinal functional impairment in diabetic retinopathy. *Biomedicines*. 2023;12(1):44.
51. Sergeys J, Etienne I, Van Hove I, et al. Longitudinal in vivo characterization of the streptozotocin-induced diabetic mouse model: focus on early inner retinal responses. *Invest Ophthalmol Vis Sci*. 2019;60(2):807–822.
52. Pardue MT, Barnes CS, Kim MK, et al. Rodent hyperglycemia-induced inner retinal deficits are mirrored in human diabetes. *Transl Vis Sci Technol*. 2014;3(3):6.
53. Araiz JJ, Alvárez-Nólting R, Miranda M, et al. Changes in the Erg of Stz induced diabetic rats and its utility to detect other cerebral alterations. *Invest Ophthalmol Vis Sci*. 2010;51(13):2464.
54. Leal EC, Martins J, Voabil P, et al. Calcium dobesilate inhibits the alterations in tight junction proteins and leukocyte adhesion to retinal endothelial cells induced by diabetes. *Diabetes*. 2010;59(10):2637–2645.
55. Voabil P, Liberal J, Leal EC, et al. Calcium dobesilate is protective against inflammation and oxidative/nitrosative stress in the retina of a type 1 diabetic rat model. *Ophthalmic Res*. 2017;58(3):150–161.

Investigative Ophthalmology & Visual Science